P- and S-wave velocity of dry, water-saturated, and frozen basalt: Implications for the interpretation of Martian seismic data

Michael Heap

P- and S-wave velocity of dry, water-saturated, and frozen basalt: Implications for the interpretation of Martian seismic data

Michael J. Heap

Géophysique Expérimentale, Institut de Physique de Globe de Strasbourg (UMR 7516 CNRS, Université de Strasbourg/EOST), 5 rue René Descartes, 67084 Strasbourg cedex, France.

Corresponding author: M.J. Heap (heap@unistra.fr)

Abstract

The theoretical predictions for the P- and S-wave velocity of basalt with pore spaces filled with gaseous CO_2, liquid water, or water ice presented herein could help improve interpretations of the seismic data collected by NASA's InSight lander, which landed on the Martian surface in November 2018.

Keywords: InSight lander; SEIS; Mars; seismic velocities; basalt

Highlights

- Velocities of porous basalt decrease as a function of increasing porosity
- Velocities of porous basalt depend on pore aspect ratio
- Velocities of water ice-saturated basalt are higher than gaseous CO_2- or liquid water-saturated basalt
- Presented modelling could improve interpretations of the seismic data collected by the InSight lander

1 Introduction

There is abundant evidence that liquid water existed on the surface of Mars in its geological past (e.g., Baker, 1979; Carr, 1996; Baker, 2001). However, the present-day Martian surface is largely dry and water is restricted to polar ice caps (e.g., Titus et al., 2003; Bibring et al., 2004; Grima et al., 2009) and the subsurface hydro- and cryosphere (e.g., Fanale et al., 1986; Clifford, 1993; Boynton et al., 2002; Mitrofanov et al., 2003; Mellon et al., 2004; Orosei et al., 2018). Since the surface temperature of Mars ranges from -150 to 20 °C, subsurface water exists as water ice or liquid water, varying with, amongst other factors, space (i.e. latitude) and time (i.e. seasonal variations) (e.g., Fanale et al., 1986; Bandfield, 2007).

NASA's InSight lander (Banerdt et al., 2013) touched down on the Martian surface on 26 November 2018. One of the aims of the InSight mission is to better understand the interior of Mars using a seismometer (Seismic Experiment for Interior Structure, SEIS; Panning et al., 2015; 2017). Since laboratory measurements and theoretical predictions show that elastic wave velocities for rock can differ depending on whether the rock is dry or saturated with either liquid water or water ice (e.g., O'Connell and Budiansky, 1974; Toksöz et al., 1976; Kahraman, 2007), the influence of saturation state on the P- and S-wave velocity of crustal rocks is therefore of interest to those tasked with using seismic data collected by SEIS to interpret the structure and physical properties (e.g., porosity) of the shallow Martian subsurface (the brittle lithosphere) and to locate marsquakes and impacts. Due to the paucity of laboratory measurements and theoretical predictions, the P- and S-wave velocity of dry, water-saturated, and frozen basalt—the most representative rock type of the Martian crust (McSween et al., 2009)—are estimated herein as a function of porosity and pore shape using scattering theory.

2 Theory

Porous basalt, a solid groundmass that hosts pores (e.g., Saar and Manga, 1999; Al-Harthi et al., 1999; Bubeck et al., 2017), can be approximated by an equivalent homogeneous medium for wavelengths that are much longer than the characteristic pore size. Assuming that the pores (represented by spheres and oblate spheroids) are randomly distributed and that the medium is isotropic, scattering theory can be used to calculate the elastic wave velocities of the equivalent medium (Kuster and Toksöz, 1974; Toksöz et al., 1976). The equivalent bulk modulus, K^*, equivalent shear modulus, μ^*, and equivalent density, ρ^*, of the equivalent homogeneous medium are given by (Kuster and Toksöz, 1974; Toksöz et al., 1976):

$$\frac{K^* - K}{3K^* + 4\mu} = \frac{1}{3} \cdot c \cdot \frac{K' - K}{3K + 4\mu} T_{iijj}, \quad (1)$$

$$\frac{\mu^* - \mu}{6\mu^*(K + 2\mu) + \mu(9K + 8\mu)} = c \frac{(\mu' - \mu)}{25\mu(3K + 4\mu)} \left[T_{ijij} - \frac{1}{3} T_{iijj} \right], \quad (2)$$

$$\rho^* = \rho(1 - c) + c\rho'. \quad (3)$$

Where K, μ, and ρ, are the bulk modulus, shear modulus, and density of the solid groundmass, respectively, and K', μ', and ρ' are the bulk modulus, shear modulus, and density of the pore-filling medium, respectively. T_{iijj} and T_{ijij} are scalar quantities that depend on the aspect ratio of the pores and the elastic properties of the groundmass and pore-filling medium (Kuster and Toksöz, 1974; Toksöz et al., 1976) and are given by:

$$T_{iijj} = \frac{3F_1}{F_2}, \quad (4)$$

$$T_{ijij} - \frac{1}{3} T_{iijj} = \frac{2}{F_3} + \frac{1}{F_4} + \frac{F_4 F_5 + F_6 F_7 - F_8 F_9}{F_2 F_4}. \quad (5)$$

Where:

$$F_1 = 1 + A \left[\frac{3}{2}(g + \phi) - R \left(\frac{3}{2} g + \frac{5}{2} \phi - \frac{4}{3} \right) \right], \quad (6)$$

$$F_2 = 1 + A\left[1 + \frac{3}{2}(g + \phi) - \frac{R}{2}(3g + 5\phi)\right] + B(3 - 4R)$$

$$+ \frac{A}{2}(A + 3B)(3 - 4R)[g + \phi - R(g - \phi + 2\phi^2)], \quad (7)$$

$$F_3 = 1 + \frac{A}{2}\left[R(2 - \phi) + \frac{(1 + \alpha^2)}{\alpha^2}g(R - 1)\right], \quad (8)$$

$$F_4 = 1 + \frac{A}{4}[3\phi + g - R(g - \phi)], \quad (9)$$

$$F_5 = A\left[R\left(g + \phi - \frac{4}{3}\right) - g\right] + B\phi(3 - 4R), \quad (10)$$

$$F_6 = 1 + A[1 + g - R(g + \phi)] + B(1 - \phi)(3 - 4R), \quad (11)$$

$$F_7 = 2 + \frac{A}{4}[9\phi + 3g - R(5\phi + 3g)] + B\phi(3 - 4R), \quad (12)$$

$$F_8 = A\left[1 - 2R + \frac{g}{2}(R - 1) + \frac{\phi}{2}(5R - 3)\right] + B(1 - \phi)(3 - 4R), \quad (13)$$

$$F_9 = A[g(R - 1) - R\phi] + B\phi(3 - 4R), \quad (14)$$

$$A = \frac{\mu'}{\mu} - 1, \quad (15)$$

$$B = \frac{1}{3}\left(\frac{K'}{K} - \frac{\mu'}{\mu}\right), \quad (16)$$

$$R = \frac{3\mu}{3K + 4\mu}, \quad (17)$$

$$\phi = \frac{\alpha}{(1 - \alpha^2)^{3/2}}\left[cos^{-1}\alpha - \alpha(1 - \alpha^2)^{1/2}\right], \quad (18)$$

$$g = \frac{\alpha^2}{1 - \alpha^2}(3\phi - 2). \quad (19)$$

The P-wave velocity, $V_p{}^*$, and S-wave velocity, $V_s{}^*$, of the equivalent homogeneous medium can then be calculated using the following expressions (Kuster and Toksöz, 1974; Toksöz et al., 1976):

$$V_p^* = \left[\frac{K^* + {}^4\!/_3\,\mu^*}{\rho^*}\right]^{1/2}, \quad (20)$$

$$V_s^* = \left[\frac{\mu^*}{\rho^*}\right]^{1/2}. \quad (21)$$

3 Model set up and considerations

The equivalent bulk modulus, equivalent shear modulus, and equivalent density of porous basalt saturated with liquid water, water ice, and gaseous CO_2 (the most abundant molecule in the present-day Martian atmosphere; Owen et al., 1977) were determined for pore aspect ratios from 0.1 to 1 (since the aspect ratio of pores within basalt on Earth can vary significantly; e.g., Bubeck et al., 2017) and for porosities from 0 to 0.2 (since the porosity of basalt on Earth can also vary; e.g., Saar and Manga, 1999) using Equations 1, 2, and 3 and the values provided in Table 1. The P- and S-wave velocities of these equivalent media were then calculated using Equations 20 and 21, respectively. The values in Table 1 were simply chosen to explore the range of possible pore fluid properties in the Martian subsurface. I highlight here that, for example, the density of CO_2 increases from 1.8 to 2.3 kg/m^3 as temperature is decreased from 20 to -40 °C (at a pressure of 0.1 MPa). CO_2 will be a liquid, with a density close to liquid water, at ~0 °C when, for example, the pressure is higher than a few megapascals and at ~-60 °C when the pressure is higher than ~1 MPa. CO_2 will be a solid at temperatures ≥ ~-80 °C. Indeed, there is evidence of frozen CO_2 on the surface of Mars and its presence is inferred for the Martian subsurface (e.g., Mitrofanov et al., 2003). Although the density of frozen CO_2 is higher than that of water ice (frozen CO_2 has a density between 1400 and 1600 kg/m^3 at ~-80 °C and water ice has a density of 980 kg/m^3 at ~-40 °C; Table 1), their bulk moduli, for example, are very similar (Table 1; Liu, 1984). Therefore, the estimated velocities for rock saturated with liquid water may approximate those for rock saturated with liquid CO_2, and the estimated velocities for water ice-saturated rock may approximate those for rock saturated with solid (i.e. frozen) CO_2. I also highlight that liquid water and water ice on Mars could contain salts (e.g., Clark and van Hart, 1981; Vaniman et al., 2004; Zorzano et al., 2009; Stillman and Grimm, 2011) that would serve to slightly increase density (the density of seawater at 0.1 MPa, for example, varies between 1020 and 1029 kg/m^3) and lower the freezing point (salt solutions at the point of saturation will freeze at ~-20 °C). I further highlight that the densities of liquid water and water ice do not increase significantly as temperature is decreased. For example, the density of liquid water increases from 998.2 kg/m^3 at 20 °C to 999.8 kg/m^3 just above the freezing temperature. For simplicity, therefore, a water density of 1000 kg/m^3 was adopted herein (Table 1).

	Density (kg/m^3)	Bulk modulus (Pa)	Shear modulus (Pa)
Solid (i.e. pore-free) basalt groundmass	2900	8.0×10^{10}	4.0×10^{10}
Liquid water (20 °C)	1000	2.2×10^{9}	0

Water ice (-40 °C)	980	8.1×10^9	3.7×10^9
Gaseous CO_2 (20 °C)	1.8	1.0×10^5	0

Table 1. Density, bulk modulus, and shear modulus for the solid groundmass of the basalt and the three pore fluids. Solid properties for basalt estimated using data from Christensen (1972). Properties of water ice at -40 °C were taken from Toksöz et al. (1976). Properties of liquid water and CO_2 are for a pressure of 0.1 MPa and a temperature of 20 °C.

4 Results

The P- and S-wave velocity of basalt saturated with gaseous CO_2, liquid water, and water ice are plotted in Figure 1 as a function of porosity. Figures 1a, 1b, and 1c show examples of the modelled curves for pore aspect ratios of 1 (i.e. a perfect sphere), 0.5, and 0.1, respectively.

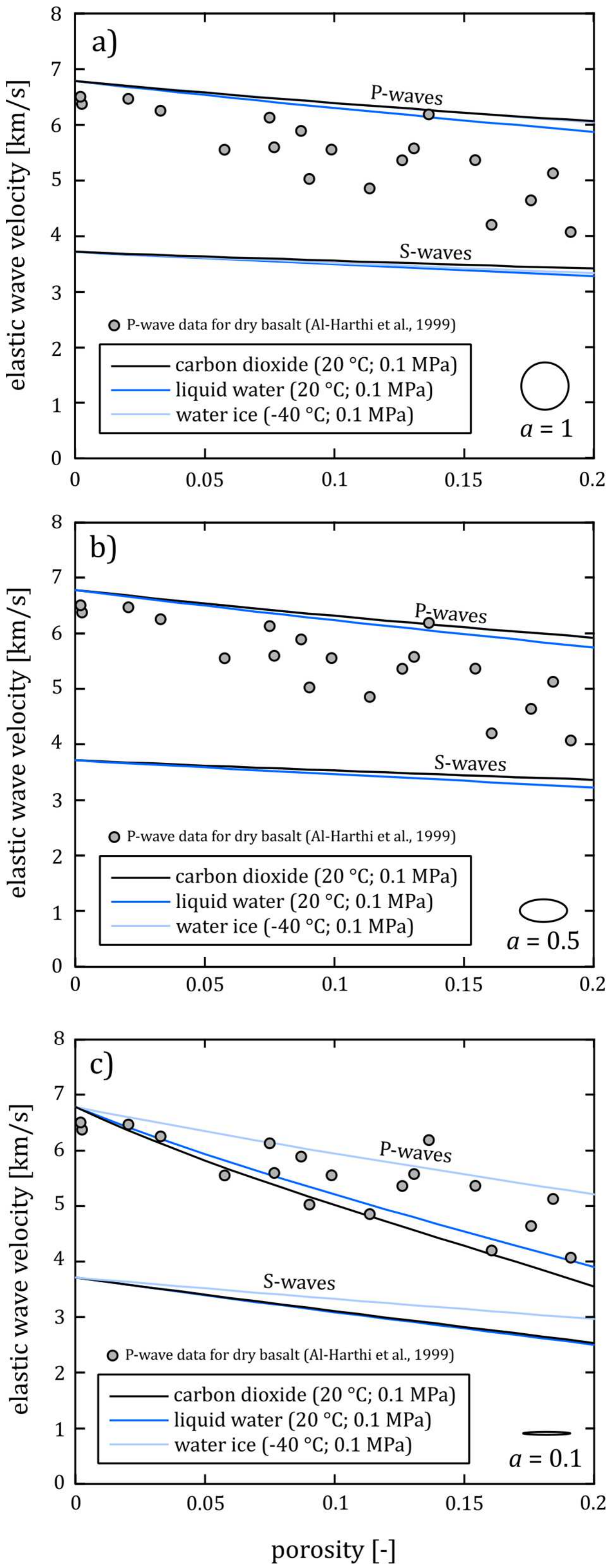

Figure 1. Elastic wave velocity (P- and S-wave velocity) of basalt as a function of porosity and saturating fluid/medium, calculated using scattering theory (see main text for details). (a) Elastic wave velocities for a basalt containing pores

with an aspect ratio of unity. (b) Elastic wave velocities for a basalt containing pores with an aspect ratio of 0.5. (c) Elastic wave velocities for a basalt containing pores with an aspect ratio of 0.1. The modelled curves are plotted alongside laboratory-measured P-wave velocity data for dry porous basalt (data from Al-Harthi et al., 1999).

The modelling shows that there are only small differences between the P- and S-wave velocities for basalts with pore aspect ratios above 0.4 (Figures 1a and 1b show modelled results for pore aspect ratios of 1 and 0.5, respectively). Below a pore aspect ratio of 0.4, the P- and S-wave velocities for basalt containing water ice within the pores are higher than those containing gaseous CO_2 and liquid water (Figure 1c shows modelled results for a pore aspect ratio 0.1).

The example shown in Figure 1c (pore aspect ratio = 0.1) shows that the P-wave velocity of basalt with pores containing water ice at a porosity of 0.2 can be more than 1 km/s higher than basalt containing liquid water, and almost 1.5 km/s higher than basalt containing gaseous CO_2. The S-wave velocity of basalt containing water ice is about 0.5 km/s higher than basalt containing either liquid water or gaseous CO_2, and the P-wave velocity of the water-saturated basalt is higher, by about 0.5 km/s, than the basalt containing gaseous CO_2, although their S-wave velocities are essentially identical (Figure 1c).

5 Discussion, implications, and conclusions

Theoretical calculations, based on scattering theory, show that the P- and S-wave velocity of frozen basalt (i.e. basalt containing water ice-filled pores) is higher than dry (containing gaseous CO_2) and water-saturated basalt when the pore aspect ratio is low (for the range of porosity values tested herein; Figure 1). These predictions are in accordance with previous observations of and theoretical predictions for ice- and water-saturated sandstone, limestone, and granite (Toksöz et al., 1976). The modelled curves of Figure 1 are plotted alongside laboratory-measured P-wave velocities for dry porous basalt (from Saudi Arabia; data from Al-Harthi et al., 1999). Not only is the P-wave velocity of the basalt with a very low porosity (a porosity of 0.002) close to the modelled curves, validating the chosen P-wave velocity for porosity-free basalt (Table 1), but the decrease as a function of porosity also closely matches that of the modelling. The comparison between these data and the modelled curves suggests that the pores within the basalt have an aspect ratio between 1.0 and 0.1 (Figure 1). Indeed, Al-Harthi et al. (1999) note that the pores in these basalts "vary in shape between being spherical and irregular, but are generally spherical".

Since low aspect ratio voids (i.e. elongated pores and fractures, the latter of which typically have an aspect ratio less than 0.01) may be commonplace in a potentially highly fractured Martian crust (e.g., Carr, 1974; MacKinnon and Tanaka, 1989; Rodríguez et al., 2005; Heap et al., 2017), and estimates for the depth of the base of the cryosphere are 2.3 and 6.5 km for the equator and poles, respectively (Clifford, 1993), it is therefore not unreasonable to expect differences in elastic wave velocities in the Martian subsurface solely as a result of the saturating fluid/medium. To assess the influence of a higher-velocity layer on the measured travel times from impacts and marsquakes, I present the results of some back-of-the-envelope calculations in Figure 2.

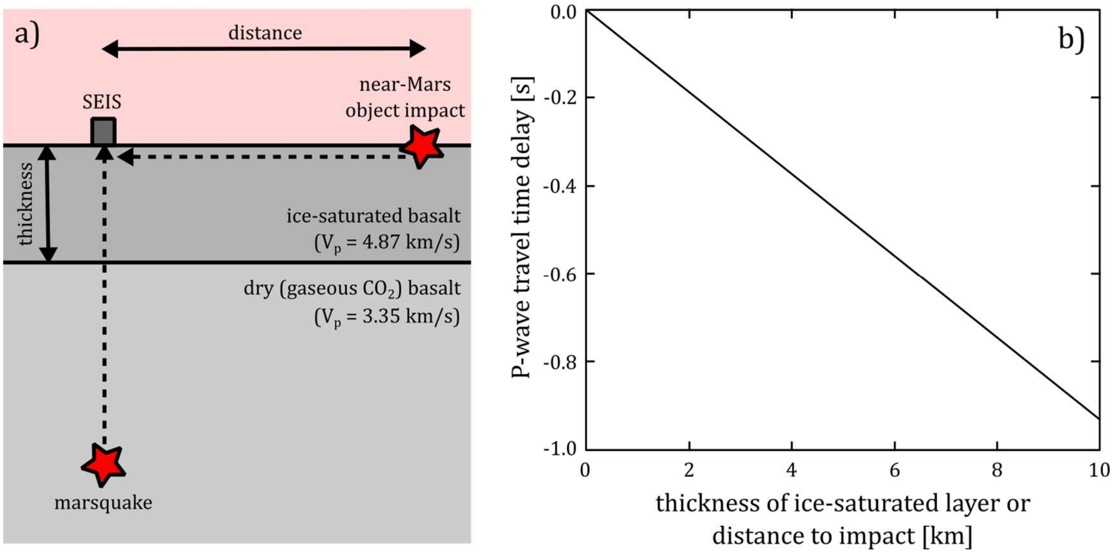

Figure 2. Back-of-the-envelope P-wave travel time delay calculations. (a) Schematic showing the simple model setup. (b) P-wave travel time delay (the difference in travel time between a Martian subsurface with and without a higher-velocity ice-saturated layer) as a function of the thickness of the ice-saturated layer (for marsquakes) or the distance to impact (for impacts).

The simple model assumes a simple subsurface structure consisting of an ice-saturated basalt layer above a dry basalt layer, both homogenous in terms of their intra-layer seismic velocities, a flat Martian surface, and direct (i.e. non-reflected) raypaths (Figure 2a). These calculations are designed to test the influence of an ice-saturated layer on the travel time delay in isolation. I highlight that there are other factors, not considered here (Figure 2), such as rock type (e.g., Lesage et al., 2018) and hydrothermal alteration (e.g., Pola et al., 2012; Mordensky et al., 2018) that are known to influence the seismic velocities of volcanic rocks. The P-wave velocities of the layers within the model are assumed to be 4.87 and 3.35 km/s for the ice-saturated and dry basalt layers, respectively (the P-wave velocities for at porosity of 0.2 and a pore aspect ratio of 0.1; Figure 1c), and therefore the travel time delay presented in Figure 2b could be considered the maximum travel time delay (i.e., the travel time delays presented here would be reduced if the porosities of the considered rock layers were reduced, for example). These simple calculations show that the travel time delay could be as much at 0.5 s for an impact even 5 km from the InSight lander, resulting in a location error of about 2 km. Based on these back-of-the-envelope calculations, the presence, and thickness, of a high-velocity ice-saturated layer could be an important consideration when using data collected by SEIS to assess the structure of the shallow Martian subsurface (the brittle lithosphere) and to locate marsquakes and impacts.

I note that the P- and S-wave velocity estimates provided herein do not take depth into account, which will serve to decrease porosity (e.g., Clifford, 1993; Wilson and Head, 1994; Heap et al., 2017) and therefore increase elastic wave velocities. However, the analysis presented herein shows that differences in P-wave velocity would be observed, in the case of low aspect ratio pores (Figure 1c), even if porosity is reduced to between 0.02-0.05, the porosity predicted for depths between 6 and 10 km (Clifford, 1993). Finally, I highlight that the small changes in pore fluid properties associated with differences in temperature (e.g., the temperature of liquid water on Mars may vary from 20 to 0.5 °C) and/or salinity (e.g., liquid water on Mars is likely to contain salts; Clark and van Hart, 1981; Vaniman et al., 2004; Zorzano et al., 2009; Stillman and Grimm, 2011) do not significantly influence the predictions presented in Figure 1. For example, the modelled curves for rock containing liquid water at a temperature of 20 °C superimpose those for rock containing liquid water at 0.5 °C.

The predictions presented herein, that elastic wave velocity depends on the void fraction and the nature of the fluid/medium within those pores, may help improve assessments of the structure of the shallow subsurface (brittle lithosphere) of Mars and place more accurate bounds on the locations of marsquake hypocentres and surface impacts detected by the SEIS instrument on the InSight lander (e.g., Teanby and Wookey, 2011). Further, if a saturating-medium is assumed, the presented modelling can be used to provide estimates of the physical properties (e.g., porosity) of the Martian subsurface. Seismic reflection and transmission coefficients (e.g., Ben-Menahem and Singh, 2012), useful for a wide range of seismological applications, could also be determined using the modelling described herein. Finally, if this method can be used to detect subsurface bodies of liquid water, it could be used to identify potentially habitable sites on Mars, or as an independent check for sites identified using other methods, such as radar (e.g., Orosei et al., 2018).

Acknowledgements

The author thanks a Prix d'Espoirs grant awarded by the University of Strasbourg. The author also acknowledges inspiring conversations with Olivier Lengliné, Paul Byrne, Sami Mikhail, Claire Cousins, Peter Grindrod, Jamie Farquharson, and Luke Griffiths. The comments of two reviewers helped improve this manuscript.

Competing interests

The author declares no competing interests.

References

Al-Harthi, A. A., Al-Amri, R. M., & Shehata, W. M. (1999). The porosity and engineering properties of vesicular basalt in Saudi Arabia. *Engineering Geology*, *54*(3-4), 313-320.

Baker, V. R. (1979). Erosional processes in channelized water flows on Mars. *Journal of Geophysical Research: Solid Earth*, *84*(B14), 7985-7993.

Baker, V. R. (2001). Water and the Martian landscape. *Nature*, *412*(6843), 228.

Bandfield, J. L. (2007). High-resolution subsurface water-ice distributions on Mars. *Nature*, *447*(7140), 64.

Banerdt, W. B., Smrekar, S., Lognonné, P., Spohn, T., Asmar, S. W., Banfield, D., ... & Giardini, D. (2013, March). InSight: a discovery mission to explore the interior of Mars. In *Lunar and planetary science conference* (Vol. 44, p. 1915).

Ben-Menahem, A., & Singh, S. J. (2012). Seismic waves and sources. Springer Science & Business Media.

Bibring, J. P., Langevin, Y., Poulet, F., Gendrin, A., Gondet, B., Berthé, M., ... & Moroz, V. (2004). Perennial water ice identified in the south polar cap of Mars. *Nature*, *428*(6983), 627.

Boynton, W. V., Feldman, W. C., Squyres, S. W., Prettyman, T. H., Brückner, J., Evans, L. G., ... & Englert, P. A. J. (2002). Distribution of hydrogen in the near surface of Mars: Evidence for subsurface ice deposits. *science*, *297*(5578), 81-85.

Bubeck, A., Walker, R. J., Healy, D., Dobbs, M., & Holwell, D. A. (2017). Pore geometry as a control on rock strength. *Earth and Planetary Science Letters*, *457*, 38-48.

Carr, M. H. (1974). Tectonism and volcanism of the Tharsis region of Mars. *Journal of Geophysical Research*, *79*(26), 3943-3949.

Carr, M. H. (1996). Water erosion on Mars and its biologic implications. *Endeavour*, *20*(2), 56-60.

Clark, B. C., & Van Hart, D. C. (1981). The salts of Mars. *Icarus*, *45*(2), 370-378.

Clifford, S. M. (1993). A model for the hydrologic and climatic behavior of water on Mars. *Journal of Geophysical Research: Planets*, *98*(E6), 10973-11016.

Fanale, F. P., Salvail, J. R., Zent, A. P., & Postawko, S. E. (1986). Global distribution and migration of subsurface ice on Mars. *Icarus*, *67*(1), 1-18.

Grima, C., Kofman, W., Mouginot, J., Phillips, R. J., Hérique, A., Biccari, D., ... & Cutigni, M. (2009). North polar deposits of Mars: Extreme purity of the water ice. *Geophysical Research Letters*, *36*(3).

Heap, M. J., Byrne, P. K., & Mikhail, S. (2017). Low surface gravitational acceleration of Mars results in a thick and weak lithosphere: Implications for topography, volcanism, and hydrology. Icarus, 281, 103-114.

Kahraman, S. (2007). The correlations between the saturated and dry P-wave velocity of rocks. *Ultrasonics*, *46*(4), 341-348.

Kuster, G. T., & Toksöz, M. N. (1974). Velocity and attenuation of seismic waves in two-phase media: Part I. Theoretical formulations. *Geophysics*, *39*(5), 587-606.

Lesage, P., Heap, M. J., & Kushnir, A. (2018). A generic model for the shallow velocity structure of volcanoes. Journal of Volcanology and Geothermal Research, 356, 114-126.

Liu, L. G. (1984). Compression and phase behavior of solid CO_2 to half a megabar. Earth and Planetary Science Letters, 71(1), 104-110.

MacKinnon, D. J., & Tanaka, K. L. (1989). The impacted Martian crust: Structure, hydrology, and some geologic implications. *Journal of Geophysical Research: Solid Earth*, *94*(B12), 17359-17370.

McSween, H. Y., Taylor, G. J., & Wyatt, M. B. (2009). Elemental composition of the Martian crust. *Science*, *324*(5928), 736-739.

Mellon, M. T., Feldman, W. C., & Prettyman, T. H. (2004). The presence and stability of ground ice in the southern hemisphere of Mars. *Icarus*, *169*(2), 324-340.

Mitrofanov, I. G., Zuber, M. T., Litvak, M. L., Boynton, W. V., Smith, D. E., Drake, D., ... & Saunders, R. S. (2003). CO2 snow depth and subsurface water-ice abundance in the northern hemisphere of Mars. *Science*, *300*(5628), 2081-2084.

Mordensky, S. P., Villeneuve, M. C., Kennedy, B. M., Heap, M. J., Gravley, D. M., Farquharson, J. I., & Reuschlé, T. (2018). Physical and mechanical property relationships of a shallow intrusion and volcanic host rock, Pinnacle Ridge, Mt. Ruapehu, New Zealand. Journal of Volcanology and Geothermal Research, 359, 1-20.

O'Connell, R. J., & Budiansky, B. (1974). Seismic velocities in dry and saturated cracked solids. *Journal of Geophysical Research*, *79*(35), 5412-5426.

Orosei, R., Lauro, S. E., Pettinelli, E., Cicchetti, A., Coradini, M., Cosciotti, B., ... & Soldovieri, F. (2018). Radar evidence of subglacial liquid water on Mars. *Science*, *361*(6401), 490-493.

Owen, T., Biemann, K., Rushneck, D. R., Biller, J. E., Howarth, D. W., & Lafleur, A. L. (1977). The composition of the atmosphere at the surface of Mars. *Journal of Geophysical research*, *82*(28), 4635-4639.

Panning, M. P., Beucler, É., Drilleau, M., Mocquet, A., Lognonné, P., & Banerdt, W. B. (2015). Verifying single-station seismic approaches using Earth-based data: Preparation for data return from the InSight mission to Mars. *Icarus*, *248*, 230-242.

Panning, M. P., Lognonné, P., Banerdt, W. B., Garcia, R., Golombek, M., Kedar, S., ... & Weber, R. (2017). Planned products of the Mars structure service for the InSight mission to Mars. *Space Science Reviews*, *211*(1-4), 611-650.

Pola, A., Crosta, G., Fusi, N., Barberini, V., & Norini, G. (2012). Influence of alteration on physical properties of volcanic rocks. Tectonophysics, 566, 67-86.

Rodríguez, J. A. P., Sasaki, S., Dohm, J. M., Tanaka, K. L., Strom, B., Kargel, J., ... & Komatsu, G. (2005). Control of impact crater fracture systems on subsurface hydrology, ground subsidence, and collapse, Mars. *Journal of Geophysical Research: Planets*, *110*(E6).

Saar, M. O., & Manga, M. (1999). Permeability-porosity relationship in vesicular basalts. *Geophysical Research Letters*, *26*(1), 111-114.

Stillman, D. E., & Grimm, R. E. (2011). Dielectric signatures of adsorbed and salty liquid water at the Phoenix landing site, Mars. *Journal of Geophysical Research: Planets*, *116*(E9).

Teanby, N. A., & Wookey, J. (2011). Seismic detection of meteorite impacts on Mars. *Physics of the Earth and Planetary Interiors*, *186*(1-2), 70-80.

Titus, T. N., Kieffer, H. H., & Christensen, P. R. (2003). Exposed water ice discovered near the south pole of Mars. *Science*, *299*(5609), 1048-1051.

Toksöz, M. N., Cheng, C. H., & Timur, A. (1976). Velocities of seismic waves in porous rocks. *Geophysics*, *41*(4), 621-645.

Vaniman, D. T., Bish, D. L., Chipera, S. J., Fialips, C. I., Carey, J. W., & Feldman, W. C. (2004). Magnesium sulphate salts and the history of water on Mars. *Nature*, *431*(7009), 663.

Wilson, L., & Head, J. W. (1994). Mars: Review and analysis of volcanic eruption theory and relationships to observed landforms. *Reviews of Geophysics*, *32*(3), 221-263.

Zorzano, M. P., Mateo-Martí, E., Prieto-Ballesteros, O., Osuna, S., & Renno, N. (2009). Stability of liquid saline water on present day Mars. *Geophysical Research Letters*, *36*(20).